Polish Society of Composite Materials
Polskie Towarzystwo Materiałów Kompozytowych

18: 1 (2018) 37-44

COMPOSITES THEORY AND PRACTICE

Marian Klasztorny[1]*, Daniel B. Nycz[2], Kamil Zając[1]

[1] Military University of Technology, ul. gen. W. Urbanowicza 2, 00-908 Warsaw, Poland
[2] Jan Grodek State Vocational High School, ul. A. Mickiewicza 21, 38-500 Sanok, Poland
**Corresponding author. E-mail: m.klasztorny@gmail.com*

Received (Otrzymano) 29.03.2018

ADVANCED DESIGN CALCULATIONS OF COMPOSITE BOX FOOTBRIDGE

The work develops the original methodology of design calculations for GFRP composite box footbridges. This methodology was applied to the original structural solution of a composite pedestrian-and-cyclist bridge with a 12.00 m span length and a 2.50 m platform width. The footbridge structure includes a number of original solutions regarding the superstructure, cross-section, bearings, reinforcement of support zones, transverse braces, balustrades, and railing post-platform connections. The design criteria for a GFRP composite footbridge were formulated based on the latest national standards for the design of footbridges made of conventional materials (steel, concrete) and the standard for the design of GFRP laminate tanks. The ultimate criterion for the composite superstructure was formulated using the Hashin-Fabric failure criterion and a global map of the effort index. Moreover, the serviceability criterion for the vertical deflections of the superstructure, pedestrian comfort criterion and global buckling criterion were developed. The advanced numerical modelling and simulations of the footbridge were carried out using MSC.Marc FE code. The modelling and simulation methodology, as well as the results of identification and validation tests published in the previous works by the authors were used. The results of simulation of the ultimate, serviceability and buckling limit states, corresponding to the adopted ply sequences of the laminates in the individual GFRP shells, are presented. Due to the fulfilment of all the criteria with significant margins, further numerical analyses of a footbridge with fewer laminations and design according to the Eurocodes are purposeful.

Keywords: GFRP composite footbridge, design, modelling, simulation

ZAAWANSOWANE OBLICZENIA PROJEKTOWE KOMPOZYTOWEJ SKRZYNKOWEJ KŁADKI PIESZEJ

Opracowano oryginalną metodykę obliczeń projektowych kompozytowych (GFRP) skrzynkowych kładek pieszych. Metodykę tę zastosowano do oryginalnego rozwiązania konstrukcyjnego kompozytowej skrzynkowej składki pieszo-rowerowej o rozpiętości 12.00 m i szerokości pomostu 2.50 m. Konstrukcja kładki zawiera szereg oryginalnych rozwiązań dotyczących konstrukcji nośnej, przekroju poprzecznego, łożysk, wzmocnienia stref podporowych, stężeń poprzecznych, balustrady, połączeń słupków balustrady z pomostem. Sformułowano kryteria projektowe kładki kompozytowej bazujące na ostatnich krajowych normach projektowania kładek z materiałów konwencjonalnych (stal, beton), normie projektowania zbiorników z laminatów poliestrowo-szklanych. Sformułowano kryterium nośności kompozytowej konstrukcji nośnej, w którym wykorzystano kryterium Hashin-Fabric oraz globalną mapę indeksu wytężenia, a ponadto kryterium użytkowalności dla ugięć pionowych konstrukcji nośnej, kryterium komfortu pieszych oraz kryterium stateczności globalnej. Przeprowadzono zaawansowane modelowanie numeryczne i symulacje za pomocą systemu MSC.Marc. W modelowaniu wykorzystano metodologię modelowania, wyniki badań identyfikacyjnych i testy walidacyjne opublikowane w poprzednich pracach autorów. Przedstawiono wyniki symulacji stanów granicznych nośności, użytkowalności i stateczności odpowiadające przyjętym sekwencjom warstw laminatów w poszczególnych powłokach. Ze względu na spełnienie wszystkich kryteriów ze znacznym zapasem celowe są dalsze analizy numeryczne kładki o mniejszej liczbie lamin oraz projektowanie według Eurokodów.

Słowa kluczowe: kładka z kompozytu polimerowego wzmocnionego włóknem szklanym, projektowanie, modelowanie, symulacja

INTRODUCTION

Foot and cyclist bridges made of GFRP composites are in the research and development phase, e.g. [1-4]. To date, no standard has been developed for the design of footbridges made of polymer-matrix composites. This paper proposes a new structural solution for a GFRP composite foot-and-cyclist bridge with a box-shaped superstructure, a 12.00 m span length and a 2.50 m platform width. The design of the footbridge is in line with the latest national bridge standards [5, 6]. The ultimate, serviceability and pedestrian comfort criteria formulated in [7] were developed and expanded to include the global buckling criterion of the superstructure. For the design calculations, 3D FE modelling was adopted using MSC.Marc FE code.

DESIGN ASSUMPTIONS, DESCRIPTION AND VISUALIZATION OF FOOTBRIDGE

The pedestrian and cyclist bridge is simply supported, made of glass-vinyl ester laminate with the fol-

lowing components: flame retardant vinyl ester resin BÜFA®-Firestop S440 (producer BÜFA Gelcoat Plus, Germany), quasi-balanced stitched fabrics BAT800 [0/90] and GBX800 [45/–45] (producer DIPEX, Slovakia). The fabrics have an 800 gsm weight, which differ only in the orientation of the fibres.

The footbridge superstructure has a box cross-section, two-sided longitudinal fall of 2% and a two-sided transverse fall of 1.67%. The footbridge consists of the top shell (TS), bottom shell (BS), bracing belts and cross stiffeners. The end cross stiffeners and middle cross stiffener were used in the form of diaphragms with flanges glued to the main shells. The composite footbridge parts are manufactured using infusion technology, post-cured in heat and glued together with NORPOL FI-184 glue (producer Reichhold, Norway). The average thickness of the adhesive joints is 2 mm. The balustrade has a height of 1.20 m. Two ply sequences were used:

a) top shell, excluding belts under balustrades, bottom shell, bracing belts, cross stiffeners:
   S444 = 4×BAT800 [0/90], 4×GBX800 [45/–45], 4×BAT800 [0/90];
   i.e., 12 laminae in all with an average thickness of 0.663 mm each, laminates with a total thickness of 7.96 mm;
b) belts under balustrades:
   S4444 = 4 BAT800 [0/90], 4 BAT800 [0/90], 4GBX 800 [45/-45], 4BAT 800 [0/90];
   i.e. 16 laminae in all with an average thickness of 0.663 mm each, laminates with a total thickness of 10.608 mm.

The overlap width is 10 cm. Technological rounding with a radius of 20 mm of laminates from the side of the mold were used.

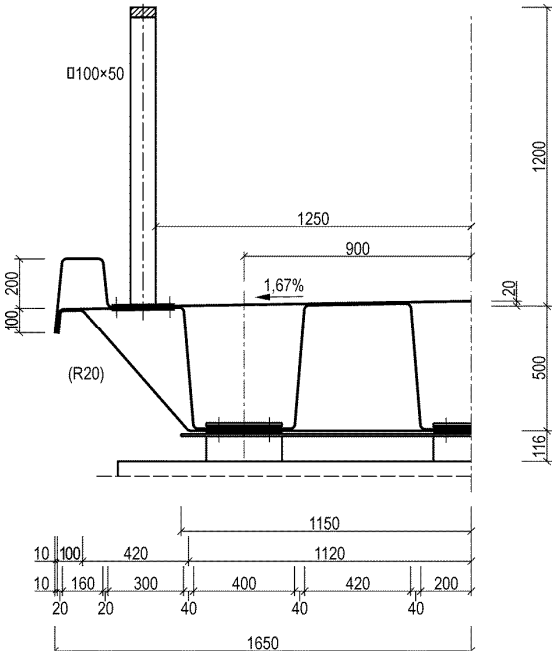

Fig. 1. GFRP composite box footbridge. Cross section at support

Rys. 1. Kładka skrzynkowa z kompozytu polimerowego wzmocnionego włóknem szklanym. Przekrój poprzeczny na podporze

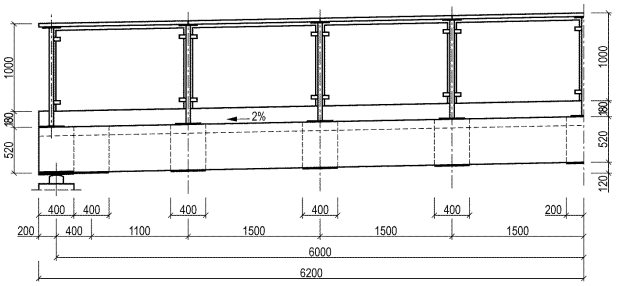

Fig. 2. GFRP composite box footbridge. Longitudinal section along the span axis

Rys. 2. Kładka skrzynkowa z kompozytu polimerowego wzmocnionego włóknem szklanym. Przekrój podłużny w osi przęsła

Figures 1 and 2 show the support cross-section and longitudinal section of the footbridge. The dimensions are given for centerlines without rounding. Six steel bearings were designed. In the support zones the BS shell is protected by 10 mm thick steel plates with rubber pads (EPDM 70° ShA, thickness 6 mm), fixed with four M16 screws. The balustrade steel posts were attached to the composite superstructure in a similar way, as indicated in Figure 3. A surface for the platform was designed in the form of spraying made of non-flammable polyurethane with an admixture of sand. The platform surface is 3 mm thick and 2.40 m wide. A wooden-polymer-steel balustrade was designed.

3D geometric modelling and visualization of the footbridge were done in the Catia v5r19 system, using Part Design, Generative Shape Design and Assembly Design. The footbridge visualization is shown in Figure 4.

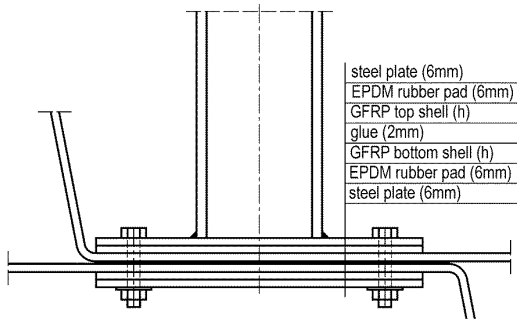

Fig. 3. GFRP composite box footbridge. Post – platform joint

Rys. 3. Kładka skrzynkowa z kompozytu polimerowego wzmocnionego włóknem szklanym. Połączenie słupka z pomostem

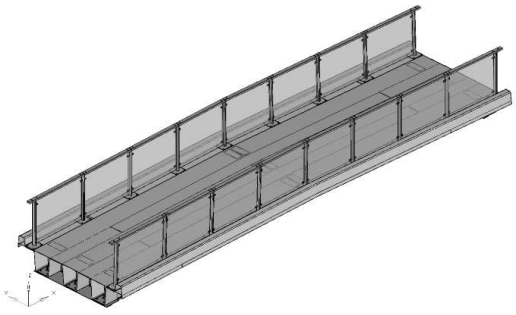

Fig. 4. GFRP composite box footbridge. Isometric top view

Rys. 4. Kładka skrzynkowa z kompozytu polimerowego wzmocnionego włóknem szklanym. Widok izometryczny z góry

SPECIFIC LOADS, DESIGN CRITERIA AND LOAD COMBINATIONS

Standards [5, 6] include only classic isotropic materials (steel, concrete, wood) and are based on ultimate limit states in which the partial safety factor method is applied. Permanent loads (self-weight, equipment weight) and variable loads (pedestrian crowd load, wind pressure) were taken into consideration.

The specific load of pedestrian crowd is vertical, evenly distributed, with an intensity of q_{kp} = 4 kN/m^2. The specific wind load is horizontal, evenly distributed, with an intensity of q_{kw1} = 1.25 kN/m^2 (loaded bridge) and q_{kw2} = 2.5 kN/m^2 (unloaded bridge). The wind pressure on the pedestrian crowd is q_{kw1} and works on a 1.70 m high field. In Ref. [7], three criteria for designing GFRP composite footbridges were formulated. The partial safety factor for GFRP composite shells in the ultimate criterion was determined in accordance with Ref. [8] which is a standard for designing GRRP composite pressure vessels. The serviceability criterion due to the vertical deflections was formulated in a similar way to that for steel footbridges. The pedestrian comfort criterion was imposed on the fundamental frequency of the footbridge based on the resonance risk levels set in Ref. [9].

In each failure criterion of a polymer-matrix laminate, the failure indices $F_i \in [0,1], i = 1,2,\ldots$ are defined, which are a measurement of the distance of the stress state at a point of the laminate superstructure from the so-called ultimate effort surface. The condition $F_i = 1$ is met on the ultimate effort surface when destruction of the laminate begins. In CAE systems, the following measures are included in addition to the failure index F_i: ≥ 1 - strength ratio (safety factor), $R_i = 1/S_i \in [0,1]$ - inverse of strength ratio, here called the effort index. Effort index R_i is an exact measurement of the distance of the stress state at each point of the laminate from the ultimate surface.

The ultimate criterion of an anisotropic GFRP laminate superstructure can be formulated in the form

$$R_{max} \leq R_u \tag{1}$$

where R_{max} is the maximum value of the effort index by all the layers of the laminate structure, $R_u = 1/S_u$ is the limit value of the effort index, S_u is the limit safety factor. The value of the S_u factor was determined on the basis of standards [5, 8]. In Ref. [8], the global safety factor is calculated from the formula

$$n = 2A_1A_2A_3A_4A_5 \tag{2}$$

where $A_i, i = 1,2,3,4,5$ are partial safety factors. In this study, the following assumptions were adopted [8]:

- The material constants of the laminae are determined experimentally on a min. of 5 samples in each strength test ($A_1 = 1.10$).
- The GFRP composite structure has full resistance to atmospheric factors and basic resistance to chemical agents ($A_2 = 1.00$).
- The design temperature is $T_D = 45$°C, and the resin heat distortion temperature is $HDT = 90$°C, hence,

$$A_3 = 1 + 0.4\,(T_D - 20)/(HDT - 40) = 1.20 \tag{3}$$

- Material fatigue is negligible due to the low number of stress cycles ($A_4 = 1.00$).
- The laminates are reinforced with E-glass roving fabrics, and the lifetime of the GFRP composite footbridge is 50 years ($A_5 = 1.90$).

For the above values of the partial safety factors the global safety factor is $n = 5.02$.

The footbridges are designed according to the partial safety factor method [5]. The minimum load factor is $\gamma_f = 1.2$, hence $S_u = n/\gamma_f = 4.18,\ R_u = 0.24$.

The serviceability criterion imposed on the vertical deflections of the footbridge has the form

$$w_{max} \leq w_u \tag{4}$$

where: w_{max} - maximum vertical deflection of the footbridge caused by the specific load of pedestrian crowd, $w_u = 1.3 \times L/300$ - permissible deflection [7]. For the footbridge with span $L = 12.00$ m, the permissible deflection is $w_u = 52$ mm.

The pedestrian comfort criterion was checked via determining the fundamental natural frequency of the unloaded footbridge (f_1) and of the footbridge loaded with a rare crowd with the intensity of 70 kg/m^2 ($f_{1,70}$). This criterion has the form [9]:

$$f_1 \geq 5.0\text{Hz}, \quad f_{1.70} \geq 2.6\text{ Hz} \tag{5}$$

In order to determine the safety factor corresponding to the global buckling of the footbridge superstructure, the eigenproblem of the footbridge under load $q_{kg} + + n_s q_{kp}$ was solved taking into account the influence of the stresses on the superstructure stiffness matrix, whereby $q_{kg} = G/A_p = 1.07$ kN/m^2 - specific dead load, $G = 32.0$ kN - total weight of the footbridge (final design result), $A_p = 30\ m^2$ - platform area, n_s - buckling factor. The n_s factor was determined using the zero fundamental natural frequency method. The calculations were made for vertical load λq_{kp}, determining the value of λ, which corresponds to $f_1 = 0$. By subtracting the influence of the permanent load, we get

$$n_s = \lambda - q_{kg}/q_{kp} = \lambda - 0.27 \tag{6}$$

The global buckling criterion has the form

$$n_s \geq n_u \tag{7}$$

where

$$n_u = 2A_1A_2A_3A_4\sqrt{A_5} \tag{8}$$

is the limit safety factor due to buckling according to Ref. [8]. For the accepted assumptions, $n_u = 3.64$ is obtained. The form of the global buckling loss corresponds to the natural mode with zero eigenfrequency.

Static calculations were performed for three load combinations [5]:

- ULS-1: permanent load
- ULS-2: permanent load plus basic variable load with a pedestrian crowd plus an additional variable load with wind (Fig. 5)
- ULS-3: permanent load plus basic variable load with wind

where: ULS - ultimate limit state. Partial load factors in the ULS states are summarized in Table 1, wherein q_{kg1} - specific vertical load corresponding to the superstructure weight, q_{kg2} - specific vertical load corresponding to the equipment weight (platform surface, balustrade).

The serviceability limit states (SLS) only consider characteristic loads, i.e. SLS-1: permanent load, SLS-2: variable load with a pedestrian crowd.

TABLE 1. **Load factors in ULS states [5]**
TABELA 1. **Współczynniki obciążenia w stanach ULS [5]**

State	q_k	γ_f
all ULS	q_{kg1}	1.2
	q_{kg2}	1.5
ULS-1	q_{kp}	1.3
ULS-2	q_{kp}	1.2
	q_{kw1}	1.2
ULS-3	q_{kw2}	1.2

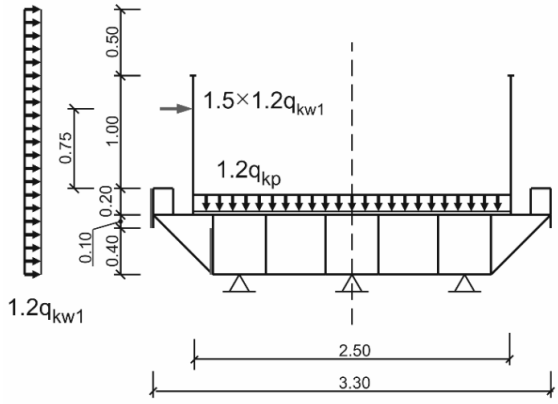

Fig. 5. Diagram of basic variable load with pedestrian crowd and additional variable load with wind in ULS-2 state [5]

Rys. 5. Schemat obciążenia podstawowego tłumem pieszych i obciążenia dodatkowego wiatrem w stanie ULS-2 [5]

GEOMETRIC AND NUMERICAL MODELLING OF FOOTBRIDGE

Geometric modelling of the footbridge was performed in the HyperMesh v12.0 system based on the fully 3D model of the footbridge. A geometric model of the footbridge, shown in Figure 6, consists of the following parts: the top shell, bottom shell, bracing belts (9 pieces), cross stiffeners (3 pieces), adhesive joints of the composite parts, steel posts (18 pieces), support steel plates (8 pieces), post fixing plates (36 pieces), rubber pads (48 pieces), screws (96 pieces). The weights of the omitted railing components have been included in the weight of the posts.

The FE mesh of the geometric model of the footbridge was created in the HyperMesh v12.0 system. The laminate shells and steel plates are meshed with four-sided QUAD4 shell elements with average dimensions of 20×20 mm. The total number of these elements is 274,272. The adhesive joints and rubber pads were meshed with HEX8 solid elements. The total number of these elements is 67,056. The screws were modelled using BAR2 beam elements each stretched between the respective steel plate nodes located in the screw axis. The total number of these elements is 96. The FE mesh in the support zone is presented in Figure 7. The tightening torques of the screws guarantee the steel plate pressure to the composite shell by means of rubber pads. It was assumed that the friction forces at the rubber pad-steel plate and rubber pad-laminate shell interfaces ensure no slip.

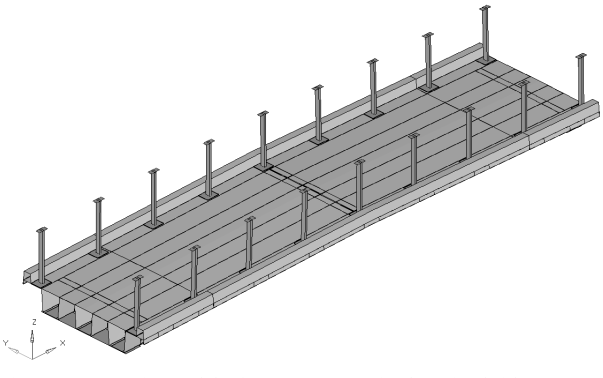

Fig. 6. Geometric model of GFRP composite box footbridge. Isometric top view

Rys. 6. Model geometryczny kładki skrzynkowej z kompozytu winylo-estrowo-szklanego. Widok izometryczny z góry

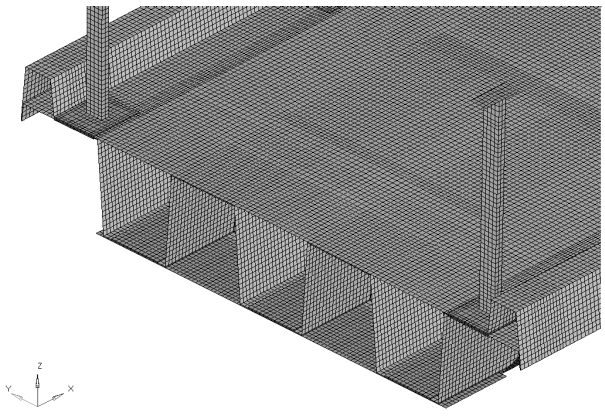

Fig. 7. FE mesh model of GFRP composite box footbridge. Isometric top view in support zone

Rys. 7. Siatka ES modelu kładki skrzynkowej z kompozytu winylo-estrowo-szklanego. Widok izometryczny z góry w strefie podporowej

Formulation of the finite elements and definition of the boundary conditions, loads, analysis options are declared in the MSC.Marc/Mentat preprocessor. The

laminate shells were meshed with 2D bilinear 4-node *Bilinear Thick-shell* finite elements (Element_75), having three translational and three rotational degrees of freedom in each node [10]. The adhesive joints were meshed with 8-node isoparametric *Three-dimensional Arbitrarily Distorted Brick* finite elements (Element_7), having three translational degrees of freedom in each node. The rubber pads were meshed with a 9-node isoparametric *Three-dimensional Arbitrarily Distorted Brick - Herrmann Formulation* finite element (Element_84). The beam elements modelling screws were assigned a 2-node *Elastic or Inelastic Beam with Transverse Shear* finite element (Element_98) [10].

The following material models were assigned to individual structural materials of the footbridge:
- lamina BG/F: orthotropic model
- NOPROL FI-184 glue, S234JR steel: isotropic model
- EPDM 70°ShA rubber: Mooney-Rivlin model.

A lamina indicated by code BG/F corresponds to one layer of fabric BAT800 [0/90] or GBX800 [45/–45] saturated with BÜFA®-Firestop S440 resin using infusion technology (lamina average thickness 0.663 mm).

After homogenization, each BG/F lamina is modelled as a linear elastic-brittle orthotropic material, with the principal directions: 1 - warp direction, 2 - weft direction, 3 - thickness direction. The effective elastic and strength constants of a lamina are as follows: E_1, E_2, E_3 - Young's modules, $\nu_{12}, \nu_{21}, \nu_{13}, \nu_{31}, \nu_{23}, \nu_{32}$ - Poisson's ratios, G_{12}, G_{13}, G_{23} - shear modules, R_{1t}, R_{2t}, R_{3t} - tensile strengths, R_{1c}, R_{2c}, R_{3c} - compressive strengths, R_{12}, R_{13}, R_{23} - shear strengths. Constant R_{13} includes destruction by delamination.

For the material model of the BG/F lamina, the *Hashin Fabric* failure model was adopted, including *Gradual Degradation* progressive destruction. The failure indices of a lamina in the *Hashin Fabric* model are defined by the equations [11]:

$$\begin{aligned}
\sigma_1 > 0: \quad & F_1 = \left(\frac{\sigma_1}{R_{1t}}\right)^2 + \left(\frac{\sigma_{12}}{R_{12}}\right)^2 + \left(\frac{\sigma_{13}}{R_{13}}\right)^2 \\
\sigma_1 < 0: \quad & F_2 = \left(\frac{\sigma_1}{R_{1c}}\right)^2 + \left(\frac{\sigma_{12}}{R_{12}}\right)^2 + \left(\frac{\sigma_{13}}{R_{13}}\right)^2 \\
\sigma_2 > 0: \quad & F_3 = \left(\frac{\sigma_2}{R_{2t}}\right)^2 + \left(\frac{\sigma_{12}}{R_{12}}\right)^2 + \left(\frac{\sigma_{23}}{R_{23}}\right)^2 \\
\sigma_2 < 0: \quad & F_4 = \left(\frac{\sigma_2}{R_{2c}}\right)^2 + \left(\frac{\sigma_{12}}{R_{12}}\right)^2 + \left(\frac{\sigma_{23}}{R_{23}}\right)^2 \\
\sigma_3 > 0: \quad & F_5 = \left(\frac{\sigma_3}{R_{3t}}\right)^2 + \left(\frac{\sigma_{12}}{R_{12}}\right)^2 + \left(\frac{\sigma_{13}}{R_{13}}\right)^2 + \left(\frac{\sigma_{23}}{R_{23}}\right)^2 \\
\sigma_3 < 0: \quad & F_6 = \left(\frac{\sigma_3}{R_{3c}}\right)^2 + \left(\frac{\sigma_{12}}{R_{12}}\right)^2 + \left(\frac{\sigma_{13}}{R_{13}}\right)^2 + \left(\frac{\sigma_{23}}{R_{23}}\right)^2
\end{aligned} \tag{9}$$

where $\sigma_1, \sigma_2, \sigma_3, \sigma_{12}, \sigma_{13}, \sigma_{23}$ - normal and shear stress components in the principal directions and planes, respectively. The strength ratios and effort indices are calculated from the formulae

$$S_i = 1/\sqrt{F_i}, \quad R_i = \sqrt{F_i}, \quad i = 1,2,\ldots,6 \tag{10}$$

For the material model of an isotropic linear elastic-brittle adhesive joint, the *Max Stress* failure model was selected. For the bilinear elastic-plastic material model of S235JR steel, the Huber-Mises-Hencky classic failure criterion was adopted.

The elastic and strength constants of BG/F lamina at room temperature, summarized in Table 2, were determined in accordance with the applicable standards [12]. The influence of the design temperature on the material constants takes into account Eq. (3). The material constants of the S235JR steel were taken from Ref. [13], and the material constants of the NORPOL FI-184 glue from the manufacturer's card (Table 3). Using the MSC.Marc/Mentat preprocessor, the average experimental tension/compression curve of the EPDM 70 ShA rubber samples was approximated and the parameter values of the 3-parameter Mooney model were determined (C_{10} = 0.457622 MPa, C_{01} = 0.719659 MPa, C_{11} = 0.0752452 MPa) as well as the bulk module B = 11773 MPa. For the rubber material the classic Huber-Mises-Hencky failure criterion was adopted.

TABLE 2. **Density and elastic and strength constants of BG/F lamina [12]**

TABELA 2. **Gęstość oraz stałe sprężystości i wytrzymałości laminy BG/F [12]**

Constant	Value
density [t/mm^3]	1.71×10^{-9}
$E_1 = E_2$ [GPa]	23.4
E_3 [GPa]	7.8
$\nu_{12} = \nu_{21}$	0.153
$\nu_{31} = \nu_{32}$	0.197
$\nu_{13} = \nu_{23}$	0.593
G_{12} [GPa]	3.5
$G_{13} = G_{23}$ [GPa]	1.4
$R_{1t} = R_{2t}$ [MPa]	449
R_{3t} [MPa]	95
$R_{1c} = R_{2c}$ [MPa]	336
R_{3c} [MPa]	348
R_{12} [MPa]	45
$R_{13} = R_{23}$ [MPa]	35

TABLE 3. **Density and elastic and strength constants of isotropic materials**

TABELA 3. **Gęstość oraz stałe sprężystości i wytrzymałości materiałów izotropowych**

Constant	Steel	Glue
Density [t/mm^3]	7.85×10^{-9}	1.14×10^{-9}
Young's modulus [GPa]	210	3.1
Tangent modulus [GPa]	1	–
Poisson's ratio	0.30	0.36
Yield strength [MPa]	372	–
$R_t = R_c$ [MPa]	–	35.0
R_s [MPa]	–	20.3

NUMERICAL ANALYSES OF FOOTBRIDGE

The static and dynamic calculations of the footbridge were performed using MSC.Marc 2010 FE code. The results of the static calculations were processed using the HyperView v12.0 system, and the results of the dynamic calculations using the MSC.Patran 2010 system. The numerical modelling and simulation were positively validated on a beam segment with the box cross-section (hat shell and plate shell glued together), subjected to the 3-point bending test [14].

Checking ultimate criterion of laminate shells

The simulations were performed for the three ULS states listed and illustrated in Section Specific loads, design criteria and load combinations. Table 4 summarizes the maximum values of effort index R_{max} of the footbridge laminate superstructure, effort index R_{max} of the adhesive joints and the Huber-Mises-Hencky reduced stress $\sigma_{red,max}$ in the steel posts and plates and rubber pads, for individual ultimate limit states. The ultimate criterion of laminate shells (1) is met. The effort level of the other components (glue, steel, rubber) is low.

TABLE 4. **Maximum values of R_{max} and $\sigma_{red,max}$**
TABELA 4. **Maksymalne wartości R_{max} oraz $\sigma_{red,max}$**

State	R_{max} laminate	R_{max} adhesive	$\sigma_{red,max}$ [MPa] steel	$\sigma_{red,max}$ [MPa] rubber
ULS-1	0.13	0.35	40.1	0.20
ULS-2	0.13	0.35	87.2	0.45
ULS-3	0.18	0.31	108.0	0.54

For example, Figures 8, 9 show a global map of effort index R presented on the midsurface of the laminate superstructure, in the ULS-2 state. The map point is the maximum value for all laminae at a given point of the midsurface. The effort maps reflect the load transfer by individual parts and allow the maximum values for design to be determined.

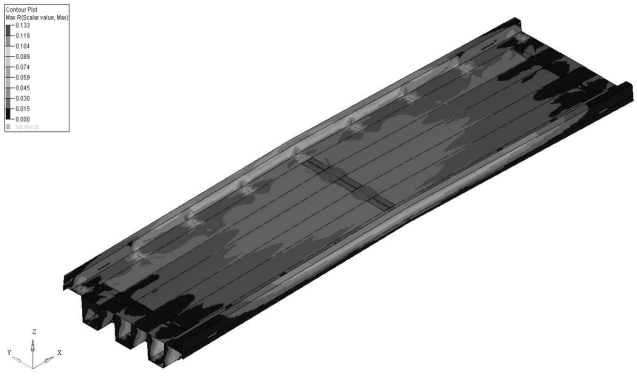

Fig. 8. Contour map of effort index R for footbridge superstructure in ULS-2 state (isometric top view)

Rys. 8. Mapa warstwicowa indeksu wytężenia R dla konstrukcji nośnej kładki w ULS-2 (widok izometryczny z góry)

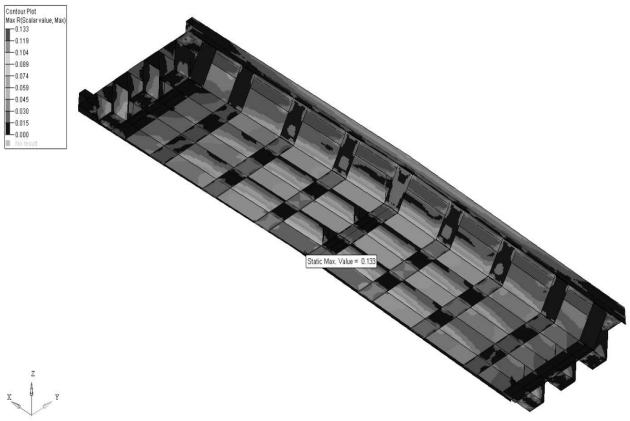

Fig. 9. Contour map of effort index R for footbridge superstructure in ULS-2 state (isometric bottom view)

Rys. 9. Mapa warstwicowa indeksu wytężenia R dla konstrukcji nośnej kładki w ULS-2 (widok izometryczny z dołu)

Checking serviceability criterion imposed on vertical deflections

The serviceability limit states SLS-1 and SLS-2 are defined in Section Specific loads, design criteria and load combinations. The contour map of the vertical displacements of the footbridge superstructure in the SLS-2 state is shown in Figure 10 in the isometric bottom view. The maximum vertical deflection in the SLS-1 state is 8.5 mm, and in the SLS-2 state 34.4 mm. Serviceability criterion (4) is met.

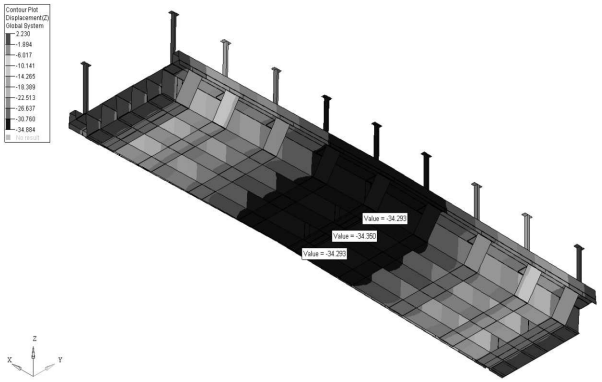

Fig. 10. Contour map of vertical displacements of footbridge superstructure in the SLS-2 state (isometric bottom view)

Rys. 10. Mapa warstwicowa przemieszczeń pionowych konstrukcji nośnej kładki w stanie SLS-2 (widok izometryczny z dołu)

Checking pedestrian comfort criterion

Modal analysis of the footbridge was carried out using the Lanczos method in the MSC.Marc system. The composite superstructure weighs 2250 kg, and the remaining parts 950 kg. A rare pedestrian crowd of the surface density of 70 kg/m^2 was mapped by a duplicate layer of finite elements on the platform, with a relatively small Young's modulus (234 MPa). The calculations were done for the footbridge without a crowd and with rare crowd. The three initial natural frequencies are listed in Table 5. Pedestrian comfort criterion (5) is met.

TABLE 5. **First three natural frequencies and modes of unloaded and loaded footbridge**
TABELA 5. **Trzy pierwsze częstotliwości własne i postacie własne kładki nieobciążonej i obciążonej**

i	f_i [Hz]	$fi_{,70}$ [Hz]	Natural mode
1	5.89	4.56	vertical flexural vibrations
2	10.28	9.34	vertical torsional vibrations
3	12.12	12.09	vertical flexural vibrations

Checking global buckling criterion

The method for global buckling analysis is described in Section Specific loads, design criteria and load combinations. Simulations of the footbridge loaded with pedestrian crowd λq_{kp} result in critical value λ, at which stability loss occurs. Then, buckling criterion (7) is checked. MSC.Marc EF code solves the eigenproblem in the form [11]:

$$[K + \lambda K_G(u, \sigma)]\phi = 0 \qquad (11)$$

where: K - stiffness matrix of the system, K_G - geometric stiffness matrix, λ - load multiplier, u - displacement, σ - stress, ϕ - eigenvector. The load multiplier at which a zero eigenfrequency appears is $\lambda = 4.603$. Using Eq. (6), one obtains

$$n_s = 4.603 - \frac{1.05}{4.0} = 4.34 > n_u = 3.88 \qquad (12)$$

Global buckling criterion (7) is met. Figure 12 shows the buckling form (modal shape) corresponding to critical load $n_s q_{kp}$.

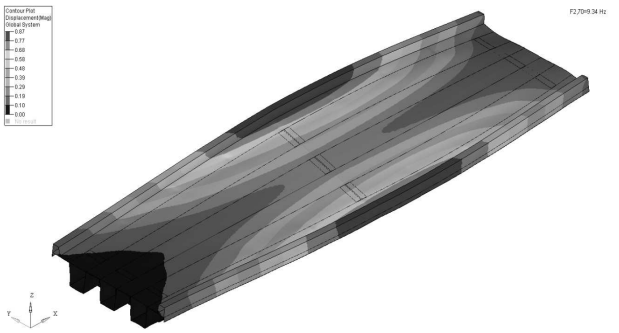

Fig. 11. Second natural mode of footbridge loaded with rare crowd
Rys. 11. Druga postać własna kładki obciążonej rzadkim tłumem

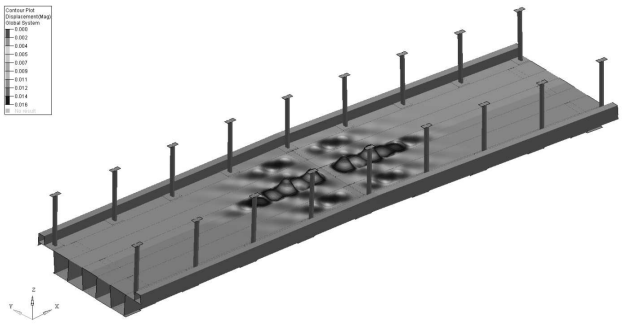

Fig. 12. Buckling form of footbridge CFB2, corresponding to first critical load (deformation scale 1000:1)
Rys. 12. Postać wyboczenia kładki CFB2, odpowiadająca pierwszemu obciążeniu krytycznemu (skala deformacji 1000:1)

CONCLUSIONS

The designed composite box footbridge is original in terms of its superstructure and equipment. The design calculations are based on 3D modelling of the composite structure in the form of glued shells. The ultimate, serviceability, pedestrian comfort and global buckling criteria for GFRP composite footbridges were developed. To check the ultimate criterion of GFRP laminate shells, an automatically generated global map of the effort index was used.

The MSC.Marc 2010 system was used for numerical modelling and simulation of the relevant static and dynamic states of the footbridge. The results of simulation of the ultimate, serviceability, pedestrian comfort and buckling limit states, corresponding to the adopted sequences of laminate layers, are presented. All the design criteria have been proven to be met. The criteria are met with significant margins, therefore it is advisable to check a footbridge with fewer composite layers and change the design according to Eurocodes.

Acknowledgements

The study has been supported by the National Centre for Research and Development, Poland, as a part of research project No. PBS1/B2/6/2013, realized in the period 2013-2015. This support is gratefully acknowledged.

REFERENCES

[1] Khalifa M.A., Hodhod O.A., Zaki M.A., Analysis and design methodology for an FRP cable-stayed pedestrian bridge, Composites: part B, 1996, 27B, 307-317.
[2] Aref A.J., Kitane Y., Lee G.C., Analysis of hybrid FRP-concrete multi-cell bridge superstructure, Composite Structures 2005, 69, 346-359.
[3] Tromp L., Composite footbridges and vacuum infusion. A 44m footbridge for Delft, Proc. 3rd Int. Conf. FOOTBRIDGE 2008, pp. 1-7.
[4] Chroscielewski J., Klasztorny M., Miskiewicz M., Romanowski R., Wilde K., Innovative design of GFRP sandwich footbridge, [In:] Footbridge 2014 5th International Conference on Footbridges: Past, Present & Future, London, England, 16-18 July 2014, USB Conf. Proceed., Paper #1250, 1-8.
[5] PN-85/S-10030. Bridge objects. Loads (in Polish).
[6] PN-82/S-10052. Bridge objects. Steel structures. Design (in Polish).
[7] Chróścielewski J., Klasztorny M., Nycz D., Sobczyk B., Loading capacity and serviceability conditions for footbridges made of fibre-reinforced polymer laminates, Roads and Bridges - Drogi i Mosty 2014, 13, 3, 189-202.
[8] PN-EN 13121-3+A1:2010E. Ground containers made of plastics reinforced with glass fibre. Part 3. Design and production control, 2010 (in Polish).
[9] Technical guide. Footbridges. Assessment of vibrational behaviour of footbridges under pedestrian loading. Setra/AFGC, Paris, France, 2006.
[10] Marc 2008 r1, Vol. B, Element Library, MSC.Software Co., Santa Ana, CA, USA.

[11] Marc 2008 r1, Vol. A, Theory and User Information, MSC.Software Co., Santa Ana, CA, USA.
[12] Klasztorny M., Nycz D.B., Romanowski R.K., Gotowicki P., Kiczko A., Rudnik D., Effects of operating temperature and accelerated environmental ageing on glass-vinylester composite mechanical properties, Mechanics of Composite Materials 2017, 53, 3, 335-350.
[13] Niezgoda T., Barnat W., Dziewulski P., Kiczko A., Numerical modelling and simulation of road crash tests with the use of advanced CAD/CAE systems, Journal of KONBiN 2012, 23, 3, 95-108.
[14] Klasztorny M., Nycz D., Cedrowski M., Modelling, simulation and validation of bending test of box segment formed as two composite shells glued together, Composites Theory and Practice 2015, 15(2), 88-94.

